Matter

CellPress

Article

A solvent-anchored non-flammable electrolyte

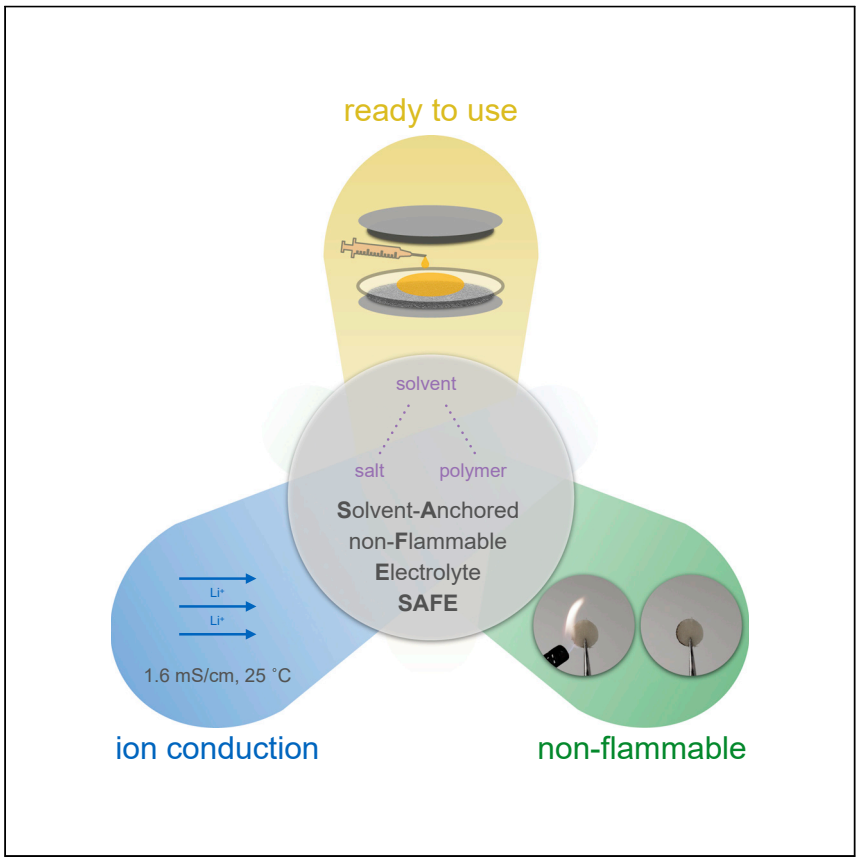

How does one use a flammable solvent to build a non-flammable electrolyte? The secret is anchoring the solvent with salts and polymers. The authors report a solvent-anchored non-flammable electrolyte (SAFE) that is ready to be paired with existing battery components. SAFE can stably operate at room temperature and has an operation range of 25°C–100°C.

Zhuojun Huang, Jian-Cheng Lai, Xian Kong, ..., Jeffrey B.-H. Tok, Yi Cui, Zhenan Bao

yicui@stanford.edu (Y.C.)
zbao@stanford.edu (Z.B.)

Highlights

A non-flammable electrolyte with ionic conductivity of 1.6 mS/cm at 25°C

Ready to use with commercially available separator and electrolyte

Ambient cycling at C/3 and C/10 with no obvious capacity decay

A wide operation range of 25°C–100°C

2 **Benchmark**
First qualification/assessment of material properties and/or performance

Huang et al., Matter 6, 445–459
February 1, 2023 © 2022 Elsevier Inc.
https://doi.org/10.1016/j.matt.2022.11.003

Matter

CellPress

Article

A solvent-anchored non-flammable electrolyte

Zhuojun Huang,[1,7] Jian-Cheng Lai,[2,7] Xian Kong,[2] Ivan Rajkovic,[3] Xin Xiao,[1] Hasan Celik,[4] Hongping Yan,[2] Huaxin Gong,[2] Paul E. Rudnicki,[2] Yangju Lin,[2] Yusheng Ye,[1] Yanbin Li,[1] Yuelang Chen,[2,5] Xin Gao,[1] Yuanwen Jiang,[2] Snehashis Choudhury,[2] Jian Qin,[2] Jeffrey B.-H. Tok,[2] Yi Cui,[1,6,*] and Zhenan Bao[2,8,*]

SUMMARY

Li-based batteries are ubiquitous in modern-day energy supply systems. However, the volatile and flammable nature of the electrolytes remains a safety challenge. Here, we report that anchored solvent molecules can increase the ionic conductivity of the electrolyte without undermining its non-flammability. Specifically, we developed a liquid-state polymer electrolyte composed of LiFSI salts, dimethoxyethane (DME) solvents, and polysiloxane tethered with ion-solvating moieties. DME coordinates with both the salt and the polymer, while, together with the salt, they synergistically plasticize the polymer to increase the ionic conductivity. The resulting non-flammable polymer electrolyte has a room-temperature ionic conductivity of 1.6 mS/cm and a wide operation window of 25°C–100°C. Benefiting from its liquid nature, our electrolyte can pair with commercially available electrodes without further cell engineering. Our work extends the ionic conductivity range of polymer electrolytes and shows a promising design pathway for next-generation safe and manufacturable electrolytes.

INTRODUCTION

Li-ion batteries (LIBs) have applications ranging from grid-level energy storage to portable consumer electronic devices.[1] However, flammability of traditional electrolytes remains a critical safety issue.[2,3] The electrolyte is usually composed of flammable small organic molecules, such as ether and carbonate. Their volatility leads to unsafe battery operation at temperatures beyond 60°C.[4] Specifically, these organic molecules undergo self-amplifying exothermic oxidation, which eventually leads to battery combustion.[2,5] Ionic-liquid-based electrolyte has been explored as a low-vapor-pressure safe electrolyte. However, these ionic liquids introduce a secondary mobile cation beyond Li^+ into the solution matrix. Due to the salt solvating limitation of ionic liquid (molar Li salt:ionic liquid $\leq$1: 2), most ($\geq$67%) of the mobile cations in the electrolyte are organic cations, instead of Li^+.[6] This results in low Li transference number (<0.4) in these electrolytes.[7]

Solid-state electrolytes, such as ceramic-based and polymer-based electrolytes, were developed as an alternative safe electrolyte.[8,9] For ceramic-based electrolytes, high Li-ion conductivities (1–10 mS/cm) have been revealed at room temperature. However, their reliance on advanced manufacturing methods, e.g., atomic-layer-deposition, for forming low-impedance interfaces with the electrodes has hindered their further development.[10] For solid-state polymeric electrolytes, low bulk ionic conductivities (<0.1 mS/cm) at room temperature have limited their operation to only elevated temperatures (60°C –80°C).[11] In full cell cycling, these electrolytes

PROGRESS AND POTENTIAL

Current battery electrolytes are flammable, posing a significant safety challenge. Solvent-free polymer electrolytes are developed to address this, yet they do not have sufficient ionic conductivity for room-temperature battery operation. Although gel electrolytes address the ionic conductivity limitation, the solvent molecules in them are not anchored and the safety feature is thus compromised. Here, we report that anchoring solvent molecules with the salt and the polymer can increase the ionic conductivity of the electrolyte without undermining its non-flammability. We name it solvent-anchored non-flammable electrolyte (SAFE). We paired SAFE with commercially available electrodes and demonstrated 400 cycles at room temperature without obvious capacity decay. Different from the polymer or gel electrolyte, SAFE addresses the apparent contradiction between non-flammability and ionic conductivity.

were also incorporated into the cathode binders to improve the ionic transport across the electrolyte-electrode interface.[12]

The limiting bulk and interfacial ionic conductivity of polymeric electrolyte is due to the coupled relationship between ionic conduction and polymer chain motion. In polymers such as poly(vinylidene fluoride)-co-hexafluoropropylene (PVDF-HFP), poly(methyl methacrylate) (PMMA), and poly(butyl acrylate) (PBuA), poly(diallyldimethylammonium) bis(fluorosulfonyl)imide (PDADFSI) increasing the salt contents shields secondary interactions between polymer chains and resulted in reduced glass transition temperatures (T_g) and elevated ionic conductivities.[12–15] However, previously used polymers, primarily based on readily commercial polymers, have rigid backbones and have limited salt solubility (maximum molar ratio salt:monomer typically <2:1). The rigid backbone restricts the polymer chain motion and thus the ionic conductivity. Although salt addition can increase the ionic conductivity, this is limited by their deficient salt solubility. In these polymer-in-salt systems, the ionic conductivity usually plateaued at ~0.1 mS/cm (25°C).[15] Another way to increase the polymer chain motion is adding organic liquids or oligomers (e.g., gel electrolyte).[16,17] However, these liquid additives can undermine the thermal stability and non-flammability of polymer electrolytes if their solvation environment and volatility is not carefully examined.

Here, we present a siloxane-based polymer, using ionic-liquid-based solvating unit as polymer side chains (solvent-anchored non-flammable electrolyte [SAFE]). The flexible low T_g backbone promotes polymer chain motion and elevates baseline ionic conductivity. By moving the ion-solvating units from the polymer backbone to the side chain, we reduce their steric hindrance and enable higher salt solubility, which further increase the ionic conductivity and decrease the viscosity of this electrolyte. Solvent molecules were incorporated into the electrolyte to maintain high ionic conductivity without affecting its non-flammability. These solvents exist in a highly coordinated environment with salts and polymers and do not undercut the safety feature of the electrolyte. To quantify and compare the solvent volatility of this and other electrolytes, we developed a gas chromatography (GC)-based measurement and found the partial vapor pressure of organic solvents in this electrolyte remains low (~2%) at high temperature (100°C) conditions.

The resulting electrolyte with high Li salt content (salt:monomer = 8:1), in presence of coordinated DME (dimethoxyethane) molecules, is a liquid with ionic conductivity of 1.6 mS/cm at 25°C. Compared with solid-state electrolytes (ceramic or polymer), SAFE easily formed intimate contact with the electrodes and can be paired with commercially available nickel-manganese-cobalt (NMC) oxide cathodes without further cell engineering. By tethering the ionic liquid units to the polymer side chain, instead of using a small-molecule ionic liquid, we limited the movement of the non-Li cation in the system and achieved a high Li transference number (~0.7). We demonstrate stable cycling of SAFE with NMC cathodes and graphite anode at 25°C (C/10 and C/3) for over 400 cycles with negligible capacity fading. This electrolyte can operate at a wide temperature range with realistic current densities (25°C, 0.27 mA/cm^2, 100°C, 5.4 mA/cm^2) and sets the conductivity and performance standards for polymer electrolytes.

RESULTS AND DISCUSSION

Materials design

We designed an amphiphilic polymeric electrolyte composed of non-polar siloxane backbone and pyrrolidinium (Py) bis(fluorosulfonyl)imide (FSI) polar ionic side

[1]Department of Materials Science and Engineering, Stanford University, Stanford, CA 94305, USA

[2]Department of Chemical Engineering, Stanford University, Stanford, CA 94305, USA

[3]Stanford Synchrotron Radiation Lightsource, SLAC National Accelerator Laboratory, Menlo Park, CA 94025, USA

[4]College of Chemistry, University of California, Berkeley, Berkley, CA 94720, USA

[5]Department of Chemistry, Stanford University, Stanford, CA 94305, USA

[6]Stanford Institute for Materials and Energy Sciences, SLAC National Accelerator Laboratory, Menlo Park, CA 94025, USA

[7]These authors contributed equally

[8]Lead contact

*Correspondence: yicui@stanford.edu (Y.C.), zbao@stanford.edu (Z.B.)

https://doi.org/10.1016/j.matt.2022.11.003

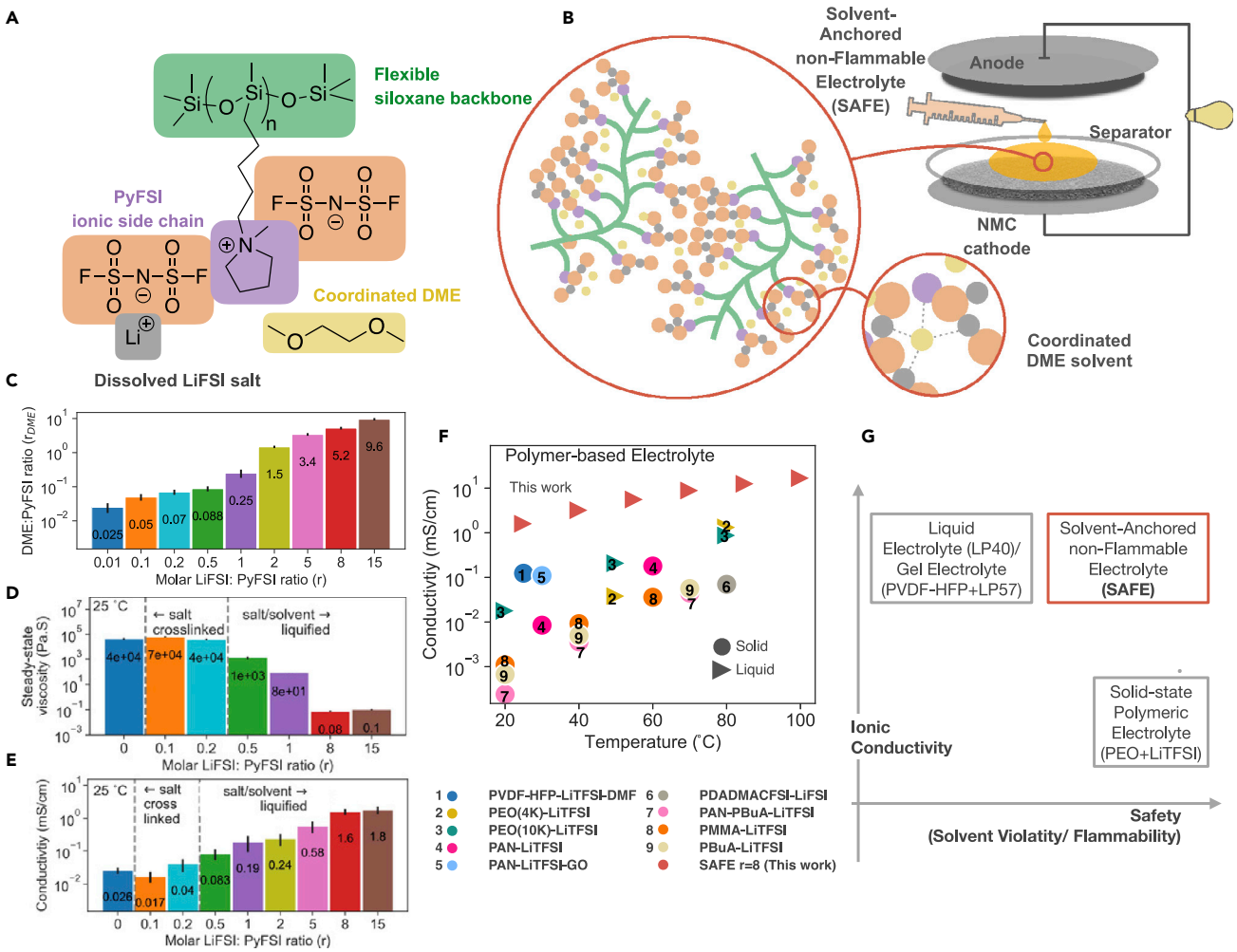

Figure 1. SAFE with different salt/solvent ratios

(A) Schematic of the chemical structure of the electrolyte drawn with the molar ratio of LiFSI:PyFSI:DME = 1:1:1.

(B) SAFE added to battery separator, and a zoom-in cartoon (drawn with the molar ratio of LiFSI:PyFSI:DME = 2:1:1.5) structure of the complex.

(C) DME amount in the electrolyte after 48 h of drying as the salt content increased. Data are represented as mean ± SD.

(D) Ionic conductivities of electrolytes with increasing salt content, measured at 25°C. Data are represented as mean ± SD.

(E) Steady-state viscosities of electrolytes. Data are represented as mean ± SD.

(F) Conductivities of SAFE r = 8 at different temperatures, and compared with other dry polymer-in-salt electrolyte.[12,13,25–29]

(G) Schematic showcasing SAFE's unique advantage.

chains, as shown in Figure 1A, and we named the polymer PPyMS-FSI. The siloxane backbone was chosen for its chemical stability and chain flexibility.[18] The PyFSI ionic group was selected for its oxidative stability and ability to solvate salt.[19,20] Other ionic-liquid-based polymer electrolytes have been studied,[21,22] especially a polymeric PyFSI ionic liquid as the polymer backbone and LiFSI (PDADFSI-LiFSI) as the salt.[15] They reported the ionic conductivity of the polymer increases with the addition of salt from r = 0.5 to r = 1.15 (PyFSI:LiFSI). At a salt:monomer ratio of 0.5 with minimal solvent presents, PDADFSI-LiFSI has an ionic conductivity of 10^{-6} mS/cm at 30°C, while our polymer electrolyte PPyMSMS-LiFSI has an ionic conductivity of 8.3×10^{-2} mS/cm at 25°C, and the higher conductivity derived from the low rigidity of the siloxane polymer backbone. In this study, by moving the ionic solvation groups to polymer side chains, we reduced the steric hindrance of the ionic liquid and increased the freedom of the PyFSI unit to coordinate with salt and

solvents (Figure 1B). Previous work also reported a polymer electrolyte with siloxane backbone tethered with imidazolium-based side chain with $\sim 10^{-3}$ mS/cm ionic conductivity at 25°C with LiTFSI:side chain = 0.03.[23] Siloxane-functioned ethers were also reported as a suitable electrolyte for LIBs, and they can pair with high-voltage cathodes when LiBOB (lithium bis(oxalato)borate) salt was used.[24]

Optimization of electrolyte composition

SAFE was prepared by dissolving the LiFSI salt in DME and PPyMS-FSI polymer in ACN (acetonitrile). After drying in a vacuum oven for 48 h, the ACN can be fully removed and the DME forms coordinated structures with polymers and salts. The residual amount was quantified with ^{1}H nuclear magnetic resonance (NMR) for electrolytes at different salt concentrations (Figures S1 and S2) and labeled as r_{DME} (molar ratio between DME and side chain) in Figure 1C. Here we note the salt content r, which is defined as the molar ratio between the added LiFSI salt and the PyFSI polymer side chain.

For the SAFE r = 8 electrolyte, we optimized the DME amount in the system by increasing the drying time from 48 to 96 and 144 h. From 48 to 96 h, the DME amount (r_{DME}) decreased from 5.25 to 2.53 (Table S1), but the viscosity increased from 0.08 Pa.S to 0.20 Pa.S (Figure S3), and the conductivity decreased from 1.6 mS/cm to 0.54 mS/cm. Further extending the drying time (144 h) resulted in salt precipitation without fully removing the DME. At 48 h of drying time, the DME in the system is optimal for reducing the viscosity and promoting the ionic conduction. The following sections will showcase that the DME exist in a highly coordinated environment with low volatility, and the electrolyte is non-flammable.

Liquid-state polymeric electrolyte

The mechanical properties and ionic conductivities of SAFE are affected not only by the solvent but also by the salt content. The steady-state viscosities (Figures 1D and S4) and the ionic conductivities (Figure 1E) of the polymeric complex at different r values were measured at 25°C. Due to the ionic nature of the PyFSI side chains, EIS (electrochemical impedance spectroscopy) measurement of the neat PPyMS-FSI polymer, a viscous liquid, showed a 2.6×10^{-2} mS/cm ionic conductivity at 25°C. When a small amount of LiFSI salt was added to the polymer matrix (i.e., r = 0.1–0.2), Li^+ established multi-coordination structures with the ionic side groups on the polymers, thereby electrostatically crosslinking the polymer chains and limiting the polymer chain motion.[25,30,31] We characterized this salt-crosslinking behavior with frequency-dependent rheology on the r = 0, r = 0.2, and r = 0.5 complex (Figure S5). Polymer with no salt (r = 0) showed liquid-like rheological property with the loss modulus (G″, liquid characteristic) higher than the storage modulus (G′, solid characteristic) across the frequency range, while r = 0.2 had a crossover between G′ and G″ at 8.5 rad/s, demonstrating viscoelastic solid-like behavior. Further increase in salt and solvent content ($r \geq 0.5$) resulted in the electrolyte becoming liquid again with G″ higher than G′ over the frequency range. The solid/liquid transition was also reflected in viscosity and ionic conductivity changes: the steady-state viscosity of the polymer/salt mixture increased from 4×10^4 Pa•S (r = 0) to 7×10^4 Pa•S (r = 0.1) and then decreased to 8×10^{-2} Pa•S (r = 8); the conductivity decreased from 2.6×10^{-2} mS/cm (r = 0) to 1.7×10^{-2} mS/cm (r = 0.1) and then increased to 1.6 mS/cm (r = 8). In our obtained differential scanning calorimetry (DSC) curves (Figure S6), the T_g of PPyMS-FSI polymer was observed at −25°C, and the SAFE r = 8 samples have T_g at −64°C, approaching the T_g of polydimethylsiloxane (PDMS) polymer without ionic interactions.[32] These results suggested that

the added LiFSI salt and DME can facilitate polymer chain motion and limit the ionic interaction between polymer side chains.[23,33]

Increasing the salt content from r = 8 to r = 15 has limited effect on the ionic conductivity. Although the r_{DME} increased from 5.2 to 9.6, the ratio between DME and LiFSI remained similar (0.65 for r = 8 and 0.64 for r = 15). At lower salt content r = 5, the ratio between DME and LiFSI is higher (0.68). This indicates that the salt solvation limit of the system has been reached at r = 8. Further increase in salt content requires the incorporation of proportional DME solvent. This is further supported by viscosity measurements, as r = 8 and r = 15 shows similar viscosity, which is orders lower than that of other electrolytes.

The ionic conductivity was next characterized over a wide temperature window from 25°C to 100°C (Figure 1F) and the obtained Nyquist plots are shown in Figure S7. Through fitting the conductivity and temperature information using the Arrhenius equation (Figure S8) for r = 8, the activation energy required for ion transport was calculated as 264 meV. When comparing the conductivities of SAFE r = 8 with other polymer-in-salt electrolytes, this electrolyte showed the highest ionic conductivities across the entire temperature range of 25°C to 100°C. Specifically, recent work on PVDF-HFP LiTFSI -based polymer-in-salt electrolyte also reported 13 wt % of residual DMF.[12] The electrolyte remained solid and demonstrated a room-temperature ionic conductivity of 0.124 mS/cm. For short-chain poly(ethylene glycol) (polyethylene oxide [PEO], molecular weight 10 K), it can also be liquefied by adding LiTFSI salt (Li:monomer = 0.125), and it has a viscosity of 55 Pa•S at 20°C. However, due to its limited ionic solvating ability, the liquefied PEO electrolyte only achieved an ionic conductivity of 0.06 mS/cm at 30°C.[25]

By tuning the LiFSI and DME amount, we preserved the ionic conductivity without compromising the safety feature of our electrolyte. SAFE simultaneously addressed the solvent flammability issue of conventional liquid/gel electrolyte and the ionic conductivity limitation of solid-state polymer electrolyte (Figure 1G).

Chemical environment of FSI, Li, and DME

The chemical coordination environment of the Li cation and the FSI anion evolved with the electrolyte's composition. Raman spectroscopy can measure the shifts in energy level of specific vibration modes of bonds, and we can then infer the changes in the chemical environment of that bond. In this system, both the ionic side chain of the polymer and the added Li salt contained the same FSI anion. As shown in Figure 2A, the vibration energy of the S–N–S bond measured for the neat PDMS-PyFSI polymer was ~711 cm^{-1}; for crystalline LiFSI salt samples it was ~762 cm^{-1}. These results were similar to literature values of the S–N–S bond Raman signals on LiFSI salt and pyrrolidinium FSI ionic liquids.[34–36] All obtained Raman spectra are shown in Figure S9. As the salt and solvent content increases, the S–N–S bond signal shifted to higher wavenumbers, indicating a more coordinated environment for the FSI anion.[37] Our Raman spectroscopy findings were further corroborated with Fourier transform infrared spectroscopy (FTIR), where we observed regions containing the S–N–S bond stretching vibration (Figures 2B and S10). As the salt content increased, the bond wavenumber in FTIR increased in the direction of Li binding with FSI, but no peak was observed at the energy of crystalline LiFSI.

Besides characterizing the FSI anions, the chemical environment of Li cations was investigated with NMR. In Figure 2C, the Li peak showed an up-field shift as the salt content in the polymer increased. The full ^{7}Li NMR spectra are shown in

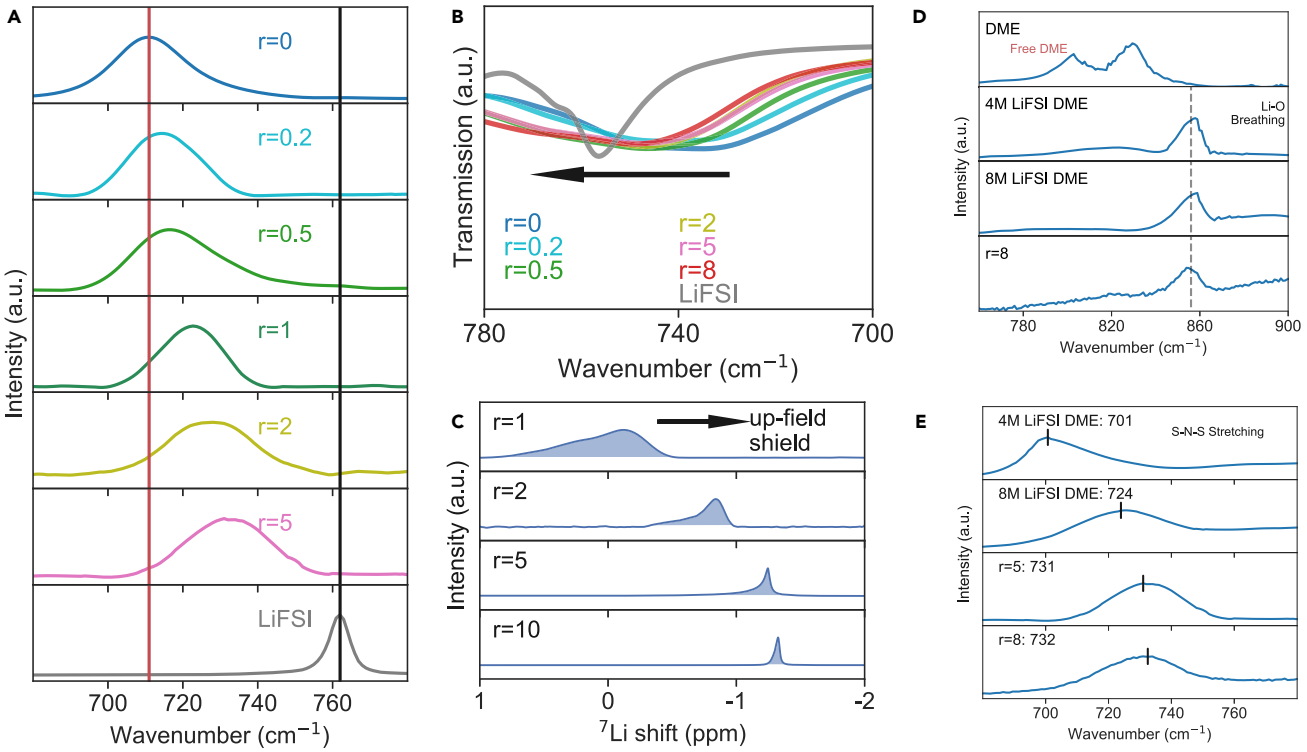

Figure 2. The coordination environment of Li^+, FSI^-, and DME

(A) Raman spectroscopy of the polymer-salt complex focused on the vibration mode of the S–N–S bond on the FSI anion.

(B) Fourier transform infrared spectroscopy (FTIR) of the polymer-salt complex focused on the signal range of the vibration mode of the S–N–S bond on the FSI anion.

(C) Li nuclear magnetic resonance (NMR) signals of polymers with various salt content measured at 25°C.

(D) Raman spectroscopy focused on DME vibration with Li–O breathing bond marked out.

(E) Raman spectroscopy focused S–N–S bond stretching compared with 4 and 8 M LiFSI DME solution (feed composition).

Figure S11. The up-field shift indicates a more shielded Li nucleus due to a higher surrounding electron cloud density. Consistent with our previous observations via Raman and FTIR, the increased salt content in the system resulted in a more coordinated solvation environment. The broadness of the NMR peak declined as the salt content increased, resulting from the lowered viscosity of the electrolyte. Furthermore, the sharp peak of Li nuclei at high salt concentration (r = 8) also indicated that the added Li salts were fully dissolved in the matrix and existed in a uniform chemical environment.

The solvation environment of the DME in SAFE was characterized with Raman spectroscopy and compared with high-concentration LiFSI DME electrolyte. Figure 2D shows the DME vibration signals. When there is no LiFSI in DME, pure DME exists in several confirmations, resulting in two distinct Raman peaks at wavenumbers lower than 850 cm^{-1}. In the 4 and 8 M LiFSI DME (feed composition) electrolytes, the Li–O breathing peak appeared at 856 cm^{-1}, indicating Li cation is coordinating with the oxygen on DME.[37] The coordination environments of the anion of the FSI anion in r = 5 and r = 8 electrolytes were also compared with 4 and 8 M LiFSI DME electrolyte (Figure 2E). When the salt concentration increased from 4 to 8 M, the peak location shifted from 701 to 724 cm^{-1}. Compared with DME electrolyte with no polymer, the S–N–S stretching in SAFE was further blue shifted to >730 cm^{-1}, indicating that the PPyMS-FSI polymer also contributed to the highly coordinated environment.

To complement experimental evidence, molecular dynamics (MD) simulations can also elucidate specific interactions in the system. We conducted MD simulations for the r = 1 electrolyte (LiFSI:PyFSI:DME = 1:1:0.25) and analyzed the radial distribution functions (RDFs) to study the interactions between the electrolyte species (Figure S12). At short range (<1 nm), a g(r) peak with a value larger than 1 indicates interaction between the two species of interest, as the local density of the selected species near the reference species is greater than its concentration in the bulk electrolyte. Li^+ shows strong interaction with both the oxygen atoms in the FSI^- and the oxygen atoms in DME, with clear peaks in the RDF. FSI^- interacts strongly with Li^+ but has no distinguishable interaction with the DME. Beside interacting with Li^+, we also find that DME interacts with the Py^+ group on the polymer side chain. Overall, our MD simulation results agree with our experimental finding that DME is anchored in a highly coordinated salt-rich environment, and DME interacts with both the Li^+ and the polymer. The potential of mean force (PMF) between any two species w(r) can be calculated from the RDF through the relation $w(r) = -k_BT \ln(g(r))$. The magnitude of the minimum of the PMF is a quantitative measurement of the interaction strength between two species. We noted that the oxygen on DME coordinates most strongly with other species and is therefore used to calculate interaction strengths for DME. We calculated PMFs for the Li^+-O (DME) and N (polymer)-O (DME) interactions and found that the Li^+-O (DME) interaction has a strength of 0.25 k_BT, while that of the N (polymer)-O (DME) interaction is 0.17 k_BT. The interaction strength of DME with the polymer is therefore slightly lower than that of DME with Li^+. Both these interactions are weaker than the ion-counterion interaction, represented by the Li^+-O (FSI^-) PMF, which has a strength of 1.30 k_BT. Therefore, these interactions likely do not strongly hinder DME or Li^+ movement in solution.

In the following section, the volatility of the solvent molecule of this electrolyte is measured and compared with other gel and high-salt-concentration electrolytes. We showed that the synergy between the salt and the polymer coordination with the solvent molecule contributes to its low volatility and the overall non-flammable nature of this electrolyte.

Stability, reactivity, and electrochemical characterizations

We selected SAFE r = 8 for further electrochemical studies since we observed that further increase in salt concentration has negligible effect on its ionic conductivity. Before applying it for long-term cycling in cells, we first examined the oxidative stability of this electrolyte in the Li|Al cell. We performed linear voltammetry on the cell and identified the oxidation voltage of SAFE r = 8 electrolyte as 6.7 V versus Li (Figure 3A). Such a high oxidative potential is sufficient for pairing with high-voltage NMC electrodes. We attributed the high oxidative stability to the electrolyte's high salt content and stable components (ionic liquids). Next, the transference number of the Li and fluorine nuclei was measured at 80°C using the diffusion ordered spectroscopy (DOSY) NMR technique. Figure S13 shows the details of the linear fitting and the calculated diffusion coefficient. The transference number of this electrolyte was computed to be 0.71, indicating that most of the mobile species in the system were Li^+. We also measured the transference number through electrochemical polarization in Li|Li symmetric cell (Figure S14), and the transference number was calculated as 0.65. This is consistent with our DOSY-NMR measurement value, and, in both measurements, we assumed that the Nernst-Einstein relationship was obeyed and the system was at the dilute limit. This is a simplified model that does not account for undissociated ion pairs/triplets, but it does offer useful insight regarding the ion movements in the electrolyte.

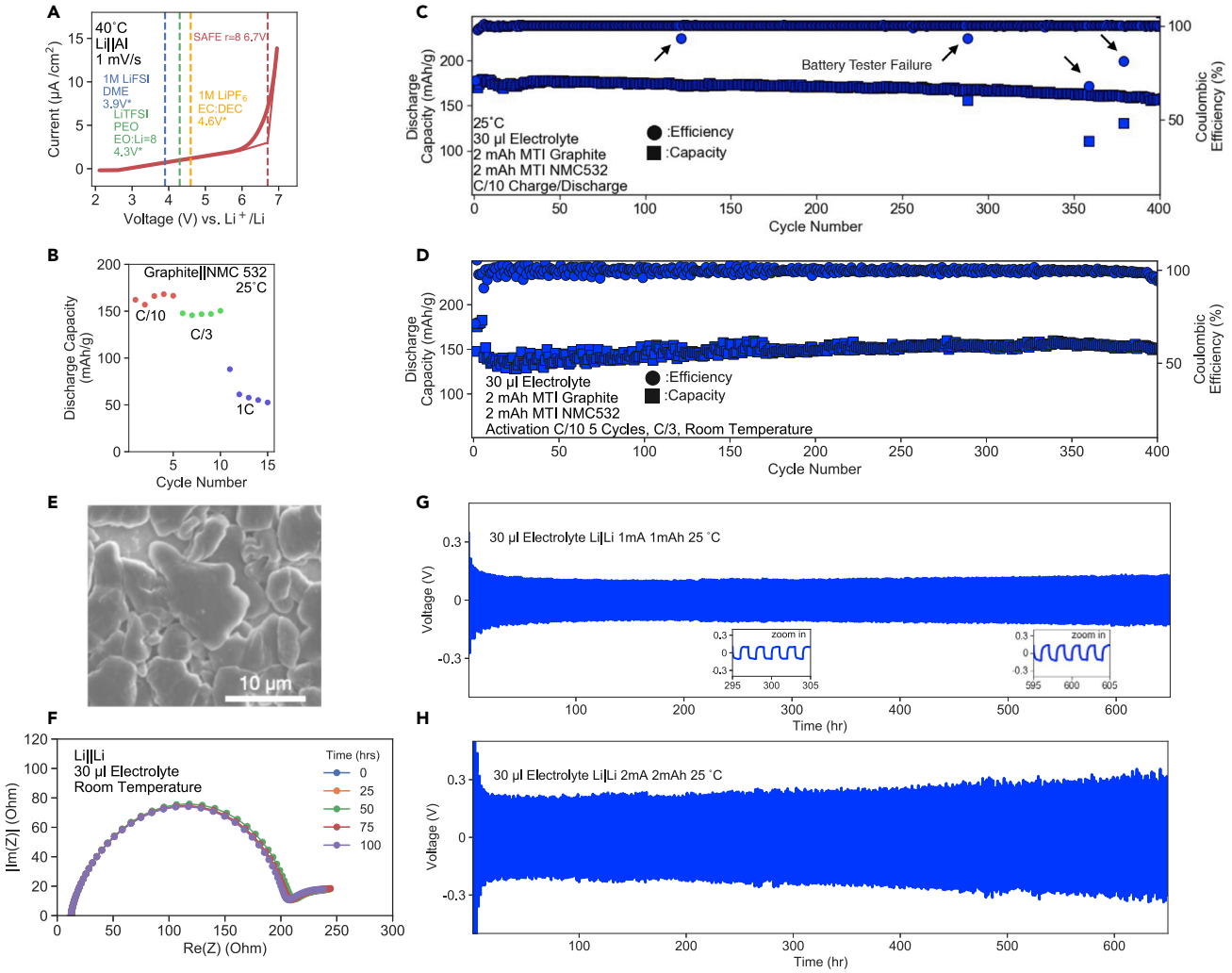

Figure 3. Stability and electrochemical characterization of SAFE r = 8

(A) Linear sweep voltammetry (LSV) performed on the electrolyte in a Li|Al cell. The measured oxidative stability is compared with that of other common polymer/liquid electrolytes.[4,38,39]

(B) Rate-dependent capacity of graphite|NMC cell.

(C) Long-term cycling of graphite|NMC cell at C/10 C-rate.

(D) Long-term cycling of graphite|NMC cell at C/3 C-rate.

(E) SEM images of Li deposition morphology (1 mAh/cm^2 capacity, 0.1 mA/cm^2 current density) on bare Cu foil. Scale bar: 10 μm.

(F) Nyquist plot of the impedance measurements on Li|Li symmetric cell with SAFE r = 8 after various resting times at room temperature.

(G) Long-term cycling of Li|Li cell at 1 mA/cm^2 current density, 1 mAh capacity.

(H) Long-term cycling of Li|Li cell at 2 mA/cm^2 current density, 2 mAh capacity.

Long-term stability and battery operation

We next examined the cycling of our electrolyte in graphite|NMC full-cell setup. The C-rate-dependent test was conducted (Figure 3B), and we found this electrolyte has ~150-mAh/g capacity at C/3 and ~170-mAh/g capacity at C/10, when pairing with commercially available NMC cathode (MTI, 2 mAh/cm^2). We cycled these graphite|NMC cells at lean electrolyte (30 μL) condition at C/10 C-rates, and we observed negligible capacity fading for over 400 cycles (Figure 3C). The voltage curves at cycle 2 and 75 were shown in Figure S15. The long-term cycling performance of two more repetitions is shown in Figure S16, and both demonstrated stable long-term performance with no observed capacity fading. For the C/3 cells, we also showed stable

long-term performance for over 400 cycles with no apparent capacity fading (Figure 3D). The fluctuation of the discharge capacities in the initial 200 cycles was attributed to the changes in the room temperature over different periods of the day, and the fluctuation was reduced once the temperature of the room was set at 25°C. Our electrolyte also demonstrated high voltage stability when cycled in a Li|LNMO cell (Figure S17).

We then evaluated the electrolyte's compatibility with Li metal anode. We deposited 1 mAh/cm^2 of Li metal on a Cu foil at a current density of 0.1 mA/cm^2. The scanning electron microscopy (SEM) deposition profiles of the Li metal (Figure 3E) indicated that the morphology of the deposited Li metal was granular and homogeneous. A zoomed-out SEM images indicated this morphology was observed over large areas on the electrodes (Figure S18). The stability of the solid-electrolyte interface (SEI) was further characterized by tracking the interfacial impedance of Li|Li symmetric cells over a prolonged period (~100 h) using EIS measurement. We observed that the interfacial impedance remained almost unchanged after resting at room temperature for 100 h, indicating that a stable interface was formed between Li metal and the electrolyte (Figure 3F). We evaluated the long-term stability of the r = 8 electrolyte with Li metal by cycling Li|Li cells at room temperature at various current densities. At current densities of 1 mA/cm^2 and capacity of 1 mAh/cm^2, SAFE r = 8 electrolytes showed a prolonged stable cycling of >700 h (Figure 3G). At a higher current density of 2 mA/cm^2 and capacity of 2 mAh/cm^2, the electrolyte demonstrated stable cycling for more than 650 h (Figure 3H).

We also characterized the chemical composition of the SEI after cycling at different C-rates for both the Li metal and the graphite anode. The graphite anode cycled at either C/10 or C/3 shared similar chemical composition, with product from salt (Li_2O, -SO_x) and solvent/polymer (-*O*-C) decomposition (Figure S19). At 1C rate, the charge/discharge process turned capacitive, and the anode surface was mostly covered with organic decomposition products (-*O*-C). A similar trend was discovered on Li metal anodes, where the anode cycled at 1C rate had significantly different surface chemistry compared with the electrode cycled at C/3 or C/10 (Figure S20). Specifically, more polymeric substance, possibly resulting from either polymer or the solvent decomposition, appeared on the anode surface, and less product derived from salt composition (Li_2O, -SO_x). Cross sections of a graphite|NMC cell were taken before and after 50 cycles (Figures S21 and S22), and SAFE r = 8 remained wetting at the electrodes and the separator after the cycling.

Thermal stability and the electrolyte's window of operation

The long-term thermal stability of the cell was investigated, where the cell was placed in a 70°C oven for prolonged periods of time, and the conductivity remained unchanged after 8 days, as shown in Figure S23. To demonstrate the effect of polymer on improving the electrolyte's thermal stability and safety feature, we also synthesized small-molecule Py12FSI ionic liquids and composed a small-molecule-based electrolyte with the same molar ratio of DME, LiFSI, and PyFSI, which we named SM. Detailed composition of the SM electrolyte is shown in Figure S24. We also compared the long-term thermal stability between the polymer and the SM electrolyte, and we found the SM electrolyte's conductivity starts to drop after 3 days of thermal hold at 70°C, while the SAFE r = 8's conductivity remained unchanged after 8 days of thermal hold (Figure S25). The thermal stability of these electrolytes was further evaluated with a flammability test. We first prepared glass wool soaked with 1 mL of either SAFE r = 8 or ethylene carbonate (EC) and diethyl carbonate (DEC) 1 M lithium hexafluorophosphate ($LiPF_6$) 10% fluoroethylene carbonate

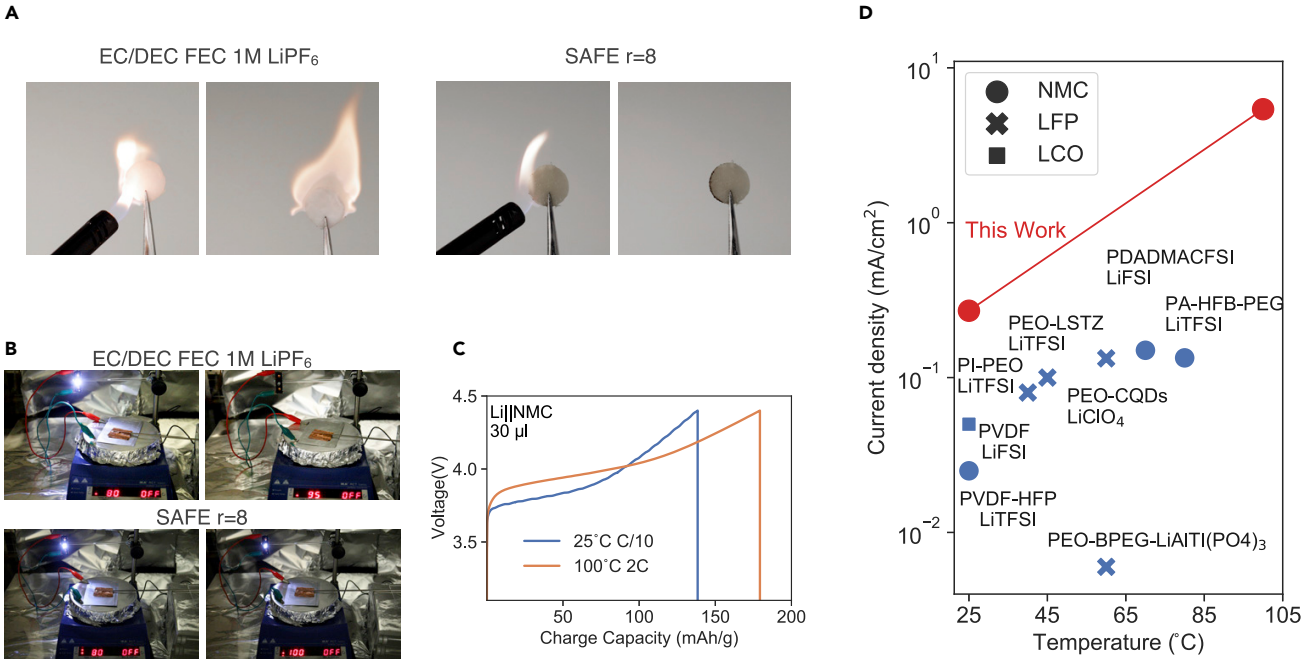

Figure 4. Thermal stability of SAFE r = 8

(A) Snapshot of glass wool soaked with 1 mL of either SAFE r = 8 or EC/DEC 1M $LiPF_6$ 10% FEC electrolyte. A flame torch was placed in contact with the glass wool for 3 s and then removed.

(B) Snapshot of pouch cell with either SAFE r = 8 or EC/DEC 1 M $LiPF_6$ 10% FEC electrolyte operating an LED light while placed on a hotplate, with the temperature of the hotplate indicated in the picture.

(C) Li|NMC cells with 30 µL of SAFE r = 8, 300 µm Li anodes, and 2.7 mAh NMC 532 Li cathodes cycled in different C-rates at 25°C.

(D) Comparison of the current density of SAFE r = 8 with other dry polymeric electrolytes in the literature.[12,15,40–46]

(FEC) electrolyte. Next, we placed a flame torch near the soaked glass wool for 3 s before removing the flame, as shown in Video S1, and snapshots of the process are shown in Figure 4A. For the carbonate electrolyte, the combustion was sustained until all the liquids were exhausted. For SAFE r = 8, only slight charring was observed on the glass wool (possibly due to salt and polymer degradation); more importantly, combustion was not sustained. In comparison, the SM electrolyte is flammable, and the combustion was sustained until all the electrolytes were burnt to a black substance (Figure S26).

Beyond flammability, we were also interested in probing the outgassing and temperature operation window of this electrolyte. Hence, we proceeded to first assemble battery pouch cells with either the SAFE r = 8 or EC/DEC 1 M $LiPF_6$ 10% FEC electrolyte. Later, the pouch cell was used to operate a light-emitting diode (LED), while being heated on a hotplate to preset desired temperatures. The collected experimental results and pictures of the camera setup are shown in Figure S27 and a snapshot of this setup is in Figure 4B. For the carbonate-based electrolyte, the LED was abruptly turned off when the hotplate was heated up to 95°C, most likely due to the loss of ionic conduction pathway in the pouch cell from electrolyte evaporation and degradation, as shown in Video S2. In contrast, the LED with the polymer-based electrolyte remained lit even after holding the hotplate temperature at 100°C for 6 min, as shown in Video S3.

We further demonstrated the thermal stability of SAFE r = 8 by recording the temperature where significant outgassing occurred. We taped the graphite|NMC pouch

Table 1. The relative saturation of solvents in different electrolytes

Type	Organic liquid electrolyte		Gel electrolyte		Ionic liquid electrolyte	SAFE	
Composition	EC/DEC 1 M LiPF6 10% FEC	4 M LiFSI DME	EC/EMC 1 M LiPF6 PVDF-HFP (50 wt % Kynar Flex 2800-00)	PC/DEC (60 wt %) LiClO4 (15 wt %) PVDF-HFP (25 wt % Kynar Flex 2800-00)	Py12FSI LiFSI DME (SM)	SAFE r = 8 (48 h)	SAFE r = 8 (96 h)
Solvent	DEC	DME	EMC	DEC	DME	DME	DME
Relative saturation @ 100°C (%)	94	84	38	80	5	2	0.6

cell to the hotplate with Kapton tapes and compared the outgassing behavior of the polymer electrolyte with EC/DEC + 10% FEC electrolyte (Figure S28). The pouch cell with the polymer electrolyte did not show outgassing until the temperature reached 160°C. At that temperature, the corners of the cell rose from the pouch inflation. For the EC/DEC electrolyte, due to the volatility of the DEC molecules, we observed the pouch cell was inflated from solvent vapor pressure starting at 105°C. We noted that significant outgassing of the polymer electrolyte happened at a temperature (160°C) higher than that of salt decomposition (140°C), indicating that salt decomposition instead of solvent outgassing is the reason for electrolyte thermal failure.

To quantify the volatility of the DME solvents in the polymer electrolyte system and to compare that with other electrolyte systems, we measured the relative saturation of different organic solvents in different electrolytes at 100°C with a GC chamber (Figure S29). By integrating the area under the curve for the solvent signal peak in the GC output and calculating the integration ratios between electrolytes and standard solvent samples, we obtained the relative saturation values, listed in Table 1. For the SAFE r = 8 electrolyte, after drying in the vacuum oven for 48 h, the relative saturation of DME was 2%. Further extending the drying to 96 h lowered the relative saturation to 0.6%. Especially, we noted the difference between this polymer liquid electrolyte and other classic gel electrolytes by measuring the relative saturation of the lowest-boiling-point component in two widely reported PVDF-HFP-based gel electrolytes.[47,48] In both cases, the relative saturations were orders higher (38%, 80%) than our reported polymer electrolyte. Similarly, we also measured the relative saturation for classic carbonate electrolyte (EC/DEC) and high-concentration ether electrolyte (4 M LiFSI DME), and we found their relative saturations were also orders higher (94%, 84%, respectively). We also found the relative saturation of DME for SM electrolyte was more than 2-fold that of SAFE r = 8 electrolyte. This series of measurements showcased that the residual DME in the polymer electrolyte has significantly lower volatility than the organic solvents in other gel, and other high-concentration (ionic-liquid based) electrolytes.

To determine the operational range and the rate capability of our polymer-based electrolyte at different temperatures, we cycled Li|NMC cells at both 25°C and 100°C to chart the rate capability of the electrolyte (Figure 4C). To reach our targeted capacity of 130 mAh/g, at 25°C, we observed that a C-rate of C/10 was needed, and, at 100°C, a C-rate of 2C was sufficient. This liquid-state polymeric electrolyte achieved a current density of 0.27 mA/cm^2 at 25°C and 5.4 mA/cm^2 at 100°C when paired with commercially available NMC cathodes. We note that our obtained current densities are compared with that of other dry polymeric electrolytes (Figure 4D)

Conclusions

In summary, we present a concept of incorporating coordinate solvent molecules into polymer electrolyte to give a non-flammable polymeric electrolyte with high

room-temperature conductivity. By employing an amphiphilic polymer design of the siloxane backbone and ionic-liquid-functioned side chains, we increased the salt solubility of the polymer. By tuning the salt and coordinated solvent content in this electrolyte, we maximized the ionic conductivity (1.6 mS/cm, 25°C) without undermining the safety feature or the thermal stability of the electrolyte. This electrolyte addresses the manufacturing difficulty of solid-state electrolyte (polymer and ceramic based) by being in the liquid state and can be readily integrated with commercially available electrodes and separators. Our electrolyte shows stable long-term operation in graphite|NMC full cell and has an operation range of 25°C to 100°C. The polymer electrolyte design concept results in a marked improvement in the ionic conductivity and manufacturability of next-generation safe polymer-based electrolytes.

EXPERIMENTAL PROCEDURES

Resource availability

Lead contact

All queries about experimental procedures can be directed to the lead contact, Zhenan Bao (zbao@stanford.edu).

Materials availability

All relevant vendors and synthesis procedures are included in the following materials section and in the supplemental information.

Data and code availability

All relevant data are included in the paper and its supplemental information.

Materials

Polymethylhydrosiloxane, trimethylsilyl terminated (PHMS, 100 mol % hydride, molecular weight, 2,100–2,400 g/mol) was purchased from Gelest. The Karstedt catalyst solution (Pt, 2% in xylene) was purchased from Santa Cruz Biotechnology. The 5-bromo-1-pentene, N-methylpyrrolidine, lithium bis(fluorosulfonyl)imide (LiFSI) and other chemicals and solvents were purchased from Sigma-Aldrich. All the chemicals were used as received without further purification. Synthesis details of the PDMS-PyFSI electrolytes are listed in the supplemental information (Figures S30–S33).

Materials characterization and simulation

Proton NMR spectra were recorded on a Bruker DRX 500 NMR spectrometer in deuterated solvents at 25°C. Li NMR spectra were recorded on Varian Inova 500 NMR spectrometer at 25°C. The chemical shift of the Li ion was compared with a standard solution of 1 M $LiClO_4$ in D_2O to evaluate the changes in Li shift relative to natural field shifting. The sample was preserved in an Ar atmosphere with epoxy sealing the NMR tube. The diffusion constants of the Li ion were measured with pulse-field gradient NMR (DOSY NMR) on a 500-MHz Bruker Avance I. The samples were prepared with a sealed D-DMSO tube inserted in the middle for shimming and locking purposes. Then the sample was sealed with a Teflon tape in an Ar environment. The DOSY-NMR measurements were carried out at the effective diffusion delay Δ = 0.5 s and the gradient pulse duration δ = 18 ms at 80°C. The signal decay was fitted to Gaussian function to extract out the diffusion constant. DSC experiments were performed using a TA Instrument Q2000 differential scanning calorimeter. The temperature range was −80°C–100°C under the heating/cooling rate of 5 °C min^{-1}. The glass transition temperature was recorded on the sample during the second heat cycle. FTIR spectra were recorded with a Nicolet iS50 FTIR spectrometer under the attenuated

total reflectance (ATR) mode. The viscosity and rheological behaviors were evaluated on a TA Instrument ARES-G2 system with a parallel plate geometry. Frequency sweeps (1–100 rad/s) were performed at 2% strain at 25°C, 35°C, and 45°C, and time-temperature superimposed to 25°C. Raman spectra were measured at 25°C on a Horiba XploRA+ confocal microscope with 532-nm laser while the polymeric electrolyte samples are sealed between two glass slides with epoxy. The conductivity of the polymeric electrolyte was measured with a biologic VMP3 system by impedance spectroscopy over a frequency range from 100 mHz to 7 MHz. The samples were sandwiched between two stainless steel spacers in a 2032 coin cell. A Teflon ring spacer with inner hole area of 0.044 cm^2 and thickness of 0.079 cm was used to confine the volume of the polymer sample. The X-ray photoelectron spectroscopy (XPS) of the deposited Li surface with PHI VersaProbe 3 using a sputtering power of 5 kV and −3′ μA, and the sample surface was sputtered with an ion beam for 1 min before the XPS spectrum was taken. MD simulation details are listed in the supplemental information (Table S2).

Cell fabrication and electrochemical characterization

All coin cell batteries were assembled in an Ar glove box kept at <0.1 ppm water and oxygen content, using 2032 coin cell geometry with 30 μL of the polymeric electrolyte and a 12 μm polyethylene (PE) separator in between. Most cells used 304 stainless steel battery casings and spacers from MTI, except cells with NMC cathode or cells for oxidation stability measurement, which used the MTI Al-Clad cathode case for high voltage stability. Li|Cu cells were assembled for XPS and SEM measurements; Li|Al cells were assembled for oxidation potential measurement; Li|Li cells were assembled for transference number measurement and long-term strip and plate cycling measurement with thick Li metal chip from MTI; Li|NMC cells were assembled with NMC 532 (2.7 mAh/cm^2 from Argonne National Laboratory) cathodes and thin (50 μm) Li metal anodes; graphite|NMC cells were assembled with NMC 532 (2.0 mAh/cm^2 from MTI) and the corresponding graphite anode. All coin cells were fabricated and rested for 24 h before cycling at an Arbin battery tester. Graphite|NMC pouch cells were assembled with NMC 532 cathode (2.0 mAh/cm^2, 25 mAh, from Argonne National Laboratory), its pairing anode, and 200 μL of electrolyte added. In coin cells, the cathodes were wetted with 10 μL of the electrolyte before the separator and the rest of the electrolyte was added. No cathode modification was performed. All pouch cells were charged to 4.0 V before being placed on a hotplate for temperature stability demonstration. The polymeric electrolyte used in all battery testing was SAFE r = 8. The liquid electrolyte used is $LiPF_6$ in EC/DEC (50/50) with 10 vol % of FEC added.

SUPPLEMENTAL INFORMATION

Supplemental information can be found online at https://doi.org/10.1016/j.matt.2022.11.003.

ACKNOWLEDGMENTS

We acknowledge support from the Assistant Secretary for Energy Efficiency and Renewable Energy, Office of Vehicle Technologies of the US Department of Energy under the Battery Materials Research (BMR) Program and Battery 500 Consortium. Part of this work was performed at the Stanford Nano Shared Facilities (SNSF), supported by the National Science Foundation under award ECCS-1542152. Z.H. acknowledges support from the American Association of University Women international fellowship and C.S. Sachse for grammar consulting. We also thank S. Nikzad and C.B. Cooper for helpful discussions.

AUTHOR CONTRIBUTIONS

Z.H., Y. Cui, and Z.B. conceived the idea. J.-C.L. designed and synthesized the polymer. Z.H. designed the experiments. Y. Cui and Z.B. directed the project. Z.H. performed material characterizations, electrochemical measurements, coin-cell and pouch-cell tests, and thermal-stability measurement. X.K. conducted the MD simulations. I.R. performed material characterization. H.C. performed DOSY-NMR experiments. X.X. performed GC measurements. H.Y. helped analyze the data. Y. Lin contributed to materials synthesis. Y.Y. manufactured the pouch cells. Y. Li, Y. Chen, H.G., and Y.J. contributed to material characterizations. P.R. helped with simulation analysis. X.G. and S.C. contributed to experimental design. J.Q. guided simulation work. J.B.-H.T. helped revise the manuscript. All authors discussed and analyzed the data. Z.H., J.-C.L., Y. Cui, and Z.B. wrote and revised the manuscript.

DECLARATION OF INTERESTS

This work has been filed as a US patent application (application no. 17/861,081).

Received: June 25, 2022
Revised: October 3, 2022
Accepted: November 3, 2022
Published: November 30, 2022

REFERENCES

1. Lin, D., Liu, Y., and Cui, Y. (2017). Reviving the lithium metal anode for high-energy batteries. Nat. Nanotechnol. *12*, 194–206. https://doi.org/10.1038/nnano.2017.16.

2. Liu, K., Liu, Y., Lin, D., Pei, A., and Cui, Y. (2018). Materials for lithium-ion battery safety. Sci. Adv. *4*, eaas9820.

3. Fan, X., Chen, L., Borodin, O., Ji, X., Chen, J., Hou, S., Deng, T., Zheng, J., Yang, C., Liou, S.-C., et al. (2018). Non-flammable electrolyte enables Li-metal batteries with aggressive cathode chemistries. Nat. Nanotechnol. *13*, 715–722. https://doi.org/10.1038/s41565-018-0183-2.

4. Kufian, M.Z., and Majid, S.R. (2010). Performance of lithium-ion cells using 1 M LiPF6 in EC/DEC (v/v = 1/2) electrolyte with ethyl propionate additive. Ionics *16*, 409–416. https://doi.org/10.1007/s11581-009-0413-6.

5. Larsson, F., Andersson, P., Blomqvist, P., and Mellander, B.-E. (2017). Toxic fluoride gas emissions from lithium-ion battery fires. Sci. Rep. *7*, 10018. https://doi.org/10.1038/s41598-017-09784-z.

6. Henderson, W.A., and Passerini, S. (2004). Phase behavior of ionic Liquid−LiX mixtures: pyrrolidinium cations and TFSI- anions. Chem. Mater. *16*, 2881–2885. https://doi.org/10.1021/cm049942j.

7. Frömling, T., Kunze, M., Schönhoff, M., Sundermeyer, J., and Roling, B. (2008). Enhanced lithium transference numbers in ionic liquid electrolytes. J. Phys. Chem. B *112*, 12985–12990. https://doi.org/10.1021/jp804097j.

8. Yu, X., and Manthiram, A. (2018). Electrode–electrolyte interfaces in lithium-based batteries. Energy Environ. Sci. *11*, 527–543.

9. Long, L., Wang, S., Xiao, M., and Meng, Y. (2016). Polymer electrolytes for lithium polymer batteries. J. Mater. Chem. *4*, 10038–10069. https://doi.org/10.1039/C6TA02621D.

10. Wang, C., Fu, K., Kammampata, S.P., McOwen, D.W., Samson, A.J., Zhang, L., Hitz, G.T., Nolan, A.M., Wachsman, E.D., Mo, Y., et al. (2020). Garnet-Type solid-state electrolytes: materials, interfaces, and batteries. Chem. Rev. *120*, 4257–4300. https://doi.org/10.1021/acs.chemrev.9b00427.

11. Murata, K., Izuchi, S., and Yoshihisa, Y. (2000). An overview of the research and development of solid polymer electrolyte batteries. Electrochim. Acta *45*, 1501–1508. https://doi.org/10.1016/S0013-4686(99)00365-5.

12. Liu, W., Yi, C., Li, L., Liu, S., Gui, Q., Ba, D., Li, Y., Peng, D., and Liu, J. (2021). Designing polymer-in-salt electrolyte and fully infiltrated 3D electrode for integrated solid-state lithium batteries. Angew. Chem. Int. Ed. *60*, 12931–12940. https://doi.org/10.1002/anie.202101537.

13. Florjańczyk, Z., Zygadło-Monikowska, E., Wieczorek, W., Ryszawy, A., Tomaszewska, A., Fredman, K., Golodnitsky, D., Peled, E., and Scrosati, B. (2004). Polymer-in-Salt electrolytes based on acrylonitrile/butyl acrylate copolymers and lithium salts. J. Phys. Chem. B *108*, 14907–14914. https://doi.org/10.1021/jp049195d.

14. Mauger, A., Julien, C.M., Paolella, A., Armand, M., and Zaghib, K. (2018). A comprehensive review of lithium salts and beyond for rechargeable batteries: progress and perspectives. Mater. Sci. Eng. R Rep. *134*, 1–21. https://doi.org/10.1016/j.mser.2018.07.001.

15. Wang, X., Chen, F., Girard, G.M.A., Zhu, H., MacFarlane, D.R., Mecerreyes, D., Armand, M., Howlett, P.C., and Forsyth, M. (2019). Poly(Ionic liquid)s-in-salt electrolytes with Co-coordination-Assisted lithium-ion transport for safe batteries. Joule *3*, 2687–2702. https://doi.org/10.1016/j.joule.2019.07.008.

16. Mackanic, D.G., Yan, X., Zhang, Q., Matsuhisa, N., Yu, Z., Jiang, Y., Manika, T., Lopez, J., Yan, H., Liu, K., et al. (2019). Decoupling of mechanical properties and ionic conductivity in supramolecular lithium ion conductors. Nat. Commun. *10*, 5384. https://doi.org/10.1038/s41467-019-13362-4.

17. Wang, Y., Zanelotti, C.J., Wang, X., Kerr, R., Jin, L., Kan, W.H., Dingemans, T.J., Forsyth, M., and Madsen, L.A. (2021). Solid-state rigid-rod polymer composite electrolytes with nanocrystalline lithium ion pathways. Nat. Mater. *20*, 1255–1263. https://doi.org/10.1038/s41563-021-00995-4.

18. Lopez, J., Pei, A., Oh, J.Y., Wang, G.J.N., Cui, Y., and Bao, Z. (2018). Effects of polymer coatings on electrodeposited lithium metal. J. Am. Chem. Soc. *140*, 11735–11744. https://doi.org/10.1021/jacs.8b06047.

19. Paillard, E., Zhou, Q., Henderson, W.A., Appetecchi, G.B., Montanino, M., and Passerini, S. (2009). Electrochemical and physicochemical properties of PY[sub 14]FSI-based electrolytes with LiFSI. J. Electrochem. Soc. *156*, A891. https://doi.org/10.1149/1.3208048.

20. Kerner, M., Plylahan, N., Scheers, J., and Johansson, P. (2015). Ionic liquid based lithium battery electrolytes: fundamental benefits of utilising both TFSI and FSI anions? Phys. Chem. Chem. Phys. *17*, 19569–19581. https://doi.org/10.1039/C5CP01891A.

21. Osada, I., de Vries, H., Scrosati, B., and Passerini, S. (2016). Ionic-liquid-based polymer

electrolytes for battery applications. Angew. Chem. Int. Ed. *55*, 500–513. https://doi.org/10.1002/anie.201504971.

22. Tripathi, A.K. (2021). Ionic liquid–based solid electrolytes (ionogels) for application in rechargeable lithium battery. Mater. Today Energy *20*, 100643. https://doi.org/10.1016/j.mtener.2021.100643.

23. Schauser, N.S., Nikolaev, A., Richardson, P.M., Xie, S., Johnson, K., Susca, E.M., Wang, H., Seshadri, R., Clément, R.J., Read de Alaniz, J., et al. (2021). Glass transition temperature and ion binding determine conductivity and lithium–ion transport in polymer electrolytes. ACS Macro Lett. *10*, 104–109. https://doi.org/10.1021/acsmacrolett.0c00788.

24. Amine, K., Wang, Q., Vissers, D.R., Zhang, Z., Rossi, N.A.A., and West, R. (2006). Novel silane compounds as electrolyte solvents for Li-ion batteries. Electrochem. Commun. *8*, 429–433. https://doi.org/10.1016/j.elecom.2005.12.017.

25. Liu, Y., Lin, D., Jin, Y., Liu, K., Tao, X., Zhang, Q., Zhang, X., and Cui, Y. (2017). Transforming from planar to three-dimensional lithium with flowable interphase for solid lithium metal batteries. Sci. Adv. *3*, eaao0713. https://doi.org/10.1126/sciadv.aao0713.

26. Yoshio, M., Nakamura, H., and Wang, H. (2009). High-energy capacitor based on graphite cathode and activated carbon anode. In Lithium-Ion Batteries, M. Yoshio, H. Nakamura, and H. Wang, eds. (Springer New York), pp. 1–8. https://doi.org/10.1007/978-0-387-34445-4_14.

27. Lascaud, S., Perrier, M., Vallee, A., Besner, S., Prud'Homme, J., and Armand, M. (1994). Phase diagrams and conductivity behavior of poly (ethylene oxide)-molten salt rubbery electrolytes. Macromolecules *27*, 7469–7477.

28. Gao, H., Grundish, N.S., Zhao, Y., Zhou, A., and Goodenough, J.B. (2021). Formation of stable interphase of polymer-in-salt electrolyte in all-solid-state lithium batteries. Adv. Energy Mater. *2021*, 1932952. https://doi.org/10.34133/2021/1932952.

29. Wu, B., Wang, L., Li, Z., Zhao, M., Chen, K., Liu, S., Pu, Y., and Li, J. (2016). Performance of "polymer-in-salt" electrolyte PAN-LiTFSI enhanced by graphene oxide filler. J. Electrochem. Soc. *163*, A2248–A2252. https://doi.org/10.1149/2.0531610jes.

30. Tirrell, M. (2018). Polyelectrolyte complexes: fluid or solid? ACS Cent. Sci. *4*, 532–533. https://doi.org/10.1021/acscentsci.8b00284.

31. Marciel, A.B., Srivastava, S., and Tirrell, M.V. (2018). Structure and rheology of polyelectrolyte complex coacervates. Soft Matter *14*, 2454–2464.

32. Clarson, S.J., Dodgson, K., and Semlyen, J.A. (1985). Studies of cyclic and linear poly(dimethylsiloxanes): 19. Glass transition temperatures and crystallization behaviour. Polymer *26*, 930–934. https://doi.org/10.1016/0032-3861(85)90140-5.

33. Chintapalli, M., Timachova, K., Olson, K.R., Mecham, S.J., Devaux, D., DeSimone, J.M., and Balsara, N.P. (2016). Relationship between conductivity, ion diffusion, and transference number in perfluoropolyether electrolytes. Macromolecules *49*, 3508–3515. https://doi.org/10.1021/acs.macromol.6b00412.

34. Huang, Q., Lee, Y.-Y., and Gurkan, B. (2019). Pyrrolidinium ionic liquid electrolyte with bis(trifluoromethylsulfonyl)imide and bis(fluorosulfonyl)imide anions: lithium solvation and mobility, and performance in lithium metal–lithium iron phosphate batteries. Ind. Eng. Chem. Res. *58*, 22587–22597. https://doi.org/10.1021/acs.iecr.9b03202.

35. Lee, S., Park, K., Koo, B., Park, C., Jang, M., Lee, H., and Lee, H. (2020). Safe, stable cycling of lithium metal batteries with low-viscosity, fire-retardant locally concentrated ionic liquid electrolytes. Adv. Funct. Mater. *30*, 2003132. https://doi.org/10.1002/adfm.202003132.

36. Haskins, J.B., Bennett, W.R., Wu, J.J., Hernández, D.M., Borodin, O., Monk, J.D., Bauschlicher, C.W., and Lawson, J.W. (2014). Computational and experimental investigation of Li-doped ionic liquid electrolytes: [pyr14][TFSI], [pyr13][FSI], and [EMIM][BF4]. J. Phys. Chem. B *118*, 11295–11309. https://doi.org/10.1021/jp5061705.

37. Yamada, Y., Yaegashi, M., Abe, T., and Yamada, A. (2013). A superconcentrated ether electrolyte for fast-charging Li-ion batteries. Chem. Commun. *49*, 11194–11196. https://doi.org/10.1039/c3cc46665e.

38. Yu, Z., Wang, H., Kong, X., Huang, W., Tsao, Y., Mackanic, D.G., Wang, K., Wang, X., Huang, W., Choudhury, S., et al. (2020). Molecular design for electrolyte solvents enabling energy-dense and long-cycling lithium metal batteries. Nat. Energy *5*, 526–533. https://doi.org/10.1038/s41560-020-0634-5.

39. Zhang, J., Zhao, N., Zhang, M., Li, Y., Chu, P.K., Guo, X., Di, Z., Wang, X., and Li, H. (2016). Flexible and ion-conducting membrane electrolytes for solid-state lithium batteries: dispersion of garnet nanoparticles in insulating polyethylene oxide. Nano Energy *28*, 447–454. https://doi.org/10.1016/j.nanoen.2016.09.002.

40. Wan, J., Xie, J., Kong, X., Liu, Z., Liu, K., Shi, F., Pei, A., Chen, H., Chen, W., Chen, J., et al. (2019). Ultrathin, flexible, solid polymer composite electrolyte enabled with aligned nanoporous host for lithium batteries. Nat. Nanotechnol. *14*, 705–711. https://doi.org/10.1038/s41565-019-0465-3.

41. He, K.-Q., Zha, J.-W., Du, P., Cheng, S.H.-S., Liu, C., Dang, Z.-M., and Li, R.K.Y. (2019). Tailored high cycling performance in a solid polymer electrolyte with perovskite-type Li0.33La0.557TiO3 nanofibers for all-solid-state lithium ion batteries. Dalton Trans. *48*, 3263–3269. https://doi.org/10.1039/C9DT00074G.

42. Ma, C., Dai, K., Hou, H., Ji, X., Chen, L., Ivey, D.G., and Wei, W. (2018). High ion-conducting solid-state composite electrolytes with carbon quantum dot nanofillers. Adv. Sci. *5*, 1700996. https://doi.org/10.1002/advs.201700996.

43. Yang, L., Zijian, W., Feng, Y., Tan, R., Zuo, Y., Gao, R., Zhao, Y., Han, L., Wang, Z., and Pan, F. (2017). Flexible composite solid electrolyte facilitating highly stable "soft contacting" Li-electrolyte interface for solid state lithium-ion batteries. Adv. Energy Mater. *7*, 1701437. https://doi.org/10.1002/aenm.201701437.

44. Xu, H., Chien, P.-H., Shi, J., Li, Y., Wu, N., Liu, Y., Hu, Y.-Y., and Goodenough, J.B. (2019). High-performance all-solid-state batteries enabled by salt bonding to perovskite in poly(ethylene oxide). Proc. Natl. Acad. Sci. USA *116*, 18815–18821. https://doi.org/10.1073/pnas.1907507116.

45. Ding, F., Xu, W., Graff, G.L., Zhang, J., Sushko, M.L., Chen, X., Shao, Y., Engelhard, M.H., Nie, Z., Xiao, J., et al. (2013). Dendrite-free lithium deposition via self-healing electrostatic shield mechanism. J. Am. Chem. Soc. *135*, 4450–4456. https://doi.org/10.1021/ja312241y.

46. Jia, M., Wen, P., Wang, Z., Zhao, Y., Liu, Y., Lin, J., Chen, M., and Lin, X. (2021). Fluorinated bifunctional solid polymer electrolyte synthesized under visible light for stable lithium deposition and dendrite-free all-solid-state batteries. Adv. Funct. Mater. *31*, 2101736. https://doi.org/10.1002/adfm.202101736.

47. Le, H.T.T., Ngo, D.T., Kalubarme, R.S., Cao, G., Park, C.-N., and Park, C.-J. (2016). Composite gel polymer electrolyte based on poly(vinylidene fluoride-hexafluoropropylene) (PVDF-HFP) with modified aluminum-doped lithium lanthanum titanate (A-LLTO) for high-performance lithium rechargeable batteries. ACS Appl. Mater. Interfaces *8*, 20710–20719. https://doi.org/10.1021/acsami.6b05301.

48. Ye, H., Huang, J., Xu, J.J., Khalfan, A., and Greenbaum, S.G. (2007). Li ion conducting polymer gel electrolytes based on ionic liquid/PVDF-HFP blends. J. Electrochem. Soc. *154*, A1048–A1057. https://doi.org/10.1149/1.2779962.